JTTEE5 18:944–956
DOI: 10.1007/s11666-009-9346-x
1059-9630/$19.00 © ASM International

Calculation of Particle Parameters for Cold Spraying of Metal-Ceramic Mixtures

S.V. Klinkov, V.F. Kosarev, A.A. Sova, and I. Smurov

(Submitted April 21, 2009; in revised form May 12, 2009)

Formation of metal-ceramic composite coatings by cold spray is one of the major directions in the development and application of the technology. As experiments showed, addition of a hard ceramic component into the mixture can shift the transition from substrate erosion to particles adhesion closer to adhesion. This effect may be induced by ceramic particles which not only erode, but also activate the target surface. Velocity and temperature of particles at their high-velocity impact onto the substrate are governing parameters in particles/substrate interaction. These parameters influence both the process of metal particles deposition and the process of erosion/activation of the substrate surface by ceramic particles. Metallic and ceramic particles collide with each other in the gas stream. These collisions can produce preactivation effect on metal particles by cleaning their surface. The level of activation depends on a typical velocity of collision which is the difference between velocities of metal and ceramic particles. Parameters of metallic and ceramic particles in the gas stream are estimated. Calculations show that components of mixtures with fine abrasive particles have greatly different velocities that influences preactivation of metal particles. At the same time, the substrate surface is activated by fine abrasive particles characterized by a high-impact velocity.

Keywords cold gas dynamic spraying, composite materials, influence of spray parameters, spray deposition

1. Introduction

Experiments showed that the interaction of metallic and abrasive particles under cold-spray conditions can lead to erosion as well as to the coating formation on the target surface (Ref 1-4). Velocity and temperature of particles at their high-velocity impact onto the substrate are governing parameters in particles/substrate interaction. Both of these parameters have effect on the process of metallic particles adhesion as well as on the process of erosion and activation at the impact of abrasive particles. It should be noted that typical stagnation temperatures of the working gas under cold-spray conditions lie within the range 300-800 K, which allows not to take into account the influence of temperature of abrasive particles, as their characteristic melting points are in the range 2000-3000 K. In this connection, it can be assumed that the effect of abrasive particles is, first of all, directed to erosion of the target surface and activation (including cleaning) of the metallic particles and target surfaces. It is necessary to note that the process of coating formation from cermet mixtures essentially differs from that employing pure metal (Ref 5-7). It is known that the deposition efficiency of cermet mixtures depends on the ratio between the components and, under certain conditions, can considerably exceed that of pure metals. At the present time, this effect is basically explained by the fact that ceramic particles, due to a high-velocity impact, rough, clean, and activate the surface thus enhancing the metal particles fixing to it and, therefore, increasing the deposition coefficient. Along with this, some quantity of ceramic particles remain in the coating (Ref 6, 8).

It may be also supposed that, apart from the activation of the substrate surface, ceramic particles produce an effect on metal particles when still moving in the gas stream. It can be assumed that moving particles of both components collide with each other. The result of such collision depends on the collision velocity, which is determined by the difference of velocities of the two moving components. Probably, several slide collisions of metallic and abrasive particles may lead to ''activation'' of the metallic particles by removal of oxide films from their surfaces.

Obviously, collisions of particles of close size and density will have no significant effect on them. On the contrary, particles with strongly different size and density will travel at considerably different speeds, and, thus, the effect of their mutual collision will be more significant. Naturally, it is impossible to definitely assert that such kind of collisions will assuredly result in the particle activation. In particular, the question of the effect of the collision orientation on the activation level, and of

S.V. Klinkov, V.F. Kosarev, and **A.A. Sova**, Khristianovich Institute of Theoretical and Applied Mechanics SB RAS (ITAM SB RAS), 630090 Novosibirsk, Russia; **S.V. Klinkov**, Novosibirsk State University, 630090 Novosibirsk, Russia; and **A.A. Sova** and **I. Smurov**, DIPI Laboratory, Ecole Nationale d'Ingénieurs de Saint-Etienne (ENISE), 58 rue Jean Parot, 420023 Saint-Etienne, France. Contact e-mail: smurov@enise.fr.

Nomenclature

a_{cr}	gas critical velocity	T_m	gas temperature at the nozzle axis
R_a	specific gas constant	λ_m	gas velocity coefficient at the nozzle axis
T	gas temperature	M_m	gas Mach number at the nozzle axis
T_0	gas stagnation temperature	U	nozzle perimeter
k	specific heat ratio	χ	effective length
a	gas sound velocity	Re_D	Reynolds number based on D
λ	velocity coefficient	M_S	Mach number after the bow shock
M	gas Mach number	z_w	compressed layer thickness
S_{cr}	critical section area	d_p	particle diameter
S	nozzle section area	m_p	particle mass
ρ	gas density	v_p	particle velocity
p	gas pressure	C_x	drag coefficient
p_0	gas stagnation pressure	S_{mid}	cross section area of the particle
δ^{**}	momentum thickness	M_p	particle Mach number
c_f	friction coefficient	Re_p	particle Reynolds number
v	gas velocity	N_m^*	number of activated metal particles
δ^*	displacement thickness	N_m	number of metal particles
z	coordinate along the nozzle axis	N_a	number of abrasive particles
δ	boundary layer thickness	v_{pm}	metal particle velocity
Re_z	Reynolds number based on z	v_{pa}	abrasive particle velocity
D	nozzle diameter	α	collision number
μ	gas viscosity	G_{pa}	abrasive particles mass flow rate
r	coordinate along the nozzle radius	d_{pm}	diameter of metal particles
G	gas flow rate	d_{pa}	diameter of abrasive particles
τ	gas tangential stress	P	probability of collision
ρ_m	gas density at the nozzle axis	I	number of collisions

how long time after collision a metallic particle can be considered as activated, remains open. However, the hypothesis of such type of activation has not been considered yet and seems to be plausible. The very first step in the assessment of such type of activation is therefore to estimate probability of the collision between metallic and ceramic particles and to evaluate characteristic impact velocities. The impact velocity between metallic and ceramic particles is strongly influenced by the location of the injection point of ceramic powder. Habitual techniques of spraying cermets deal with powder mixtures prepared prior to spraying. However, an alternative method may be proposed where metallic particles are injected into the nozzle prechamber and ceramic particles in the supersonic part of the nozzle through a separate injection point. In this case, mixing powders occur directly in the supersonic part (Ref 9).

In this paper, a numerical model for the estimation of the probability of collision between metallic and ceramic particles moving inside the nozzle at different parameters (particle concentration, particle size, etc.) of multiphase flow is proposed. To accomplish this task, it is necessary to know velocity of metallic and abrasive particles in the gas stream, which requires knowing parameters of the gas stream.

The effect of the ceramic component on the coating properties is beyond the scope of this paper, and so it is not analyzed here.

Hence, the first step will be to calculate the gas flow, then the particle velocity, and, finally, the probability of particle collisions.

2. Simulation of Gas Flow and Particle Velocity

At the present time, the software FLUENT is commonly used to calculate the gas flow (Ref 10-12). However, flow modeling by FLUENT in application to relatively long nozzles that are characteristic of cold spray, is time-costly and can take several hours. At the same time, it is often not the gas flow parameters that are of prime importance in cold spray, but parameters of the sprayed particles, their temperature, their velocity at the nozzle exit (for comparison with experimental measurements), and at the impact on the substrate surface (for assessment of the probability of coating formation). Another frequent task is to determine the optimum geometry of the acceleration nozzle, the location of the point of powder injection (for one or more powders), gas stagnation parameters (temperature and pressure) as well as the type of gas. In this case, a series of calculations of the particle velocity must be performed with varying parameters. In this kind of optimization problems, it is often required to rapidly assess the effect of one or

another parameter or the geometric dimensions of the acceleration path (i.e., entire distance traveled by the particle from the point of injection up to the impact on the substrate surface). A model and corresponding software for performing such calculations rapidly and with sufficient accuracy is the subject of the present study.

2.1 Basis of the Numerical Model of the Gas Flow

The so-called isentropic formulae can be used as an approximation for calculation of gas parameters inside a Laval nozzle (Ref 13-15). These formulas are obtained on the base of the conservation laws: enthalpy, gas dynamics and entropy, and the ideal gas state equation. Here only the case of one-dimensional flow is considered, i.e., gas parameters depend only on the longitudinal coordinate.

A Laval nozzle is a tube that is pinched in the middle, making an hourglass-shape having a converging and a diverging channel. In the narrowest place of the nozzle (channel conjunction), called the critical section, has a certain defined area (or diameter) S_{cr}. Then, the shape of the converging and diverging parts is given. The converging part is usually a cone with a barrel of a constant cross section, or its shape is given by a special profile $S(z)$, where z is the longitudinal coordinate with the origin in the converging part. Instead of the absolute flow velocity of a gas, it is customary in gas dynamics to employ the velocity coefficient λ that is the relationship between the absolute gas velocity and its critical velocity a_{cr}, which is determined by the local stagnation gas temperature T_0 and given by the formula

$$a_{cr} = \sqrt{\frac{2k}{k+1} R_a T_0}. \quad \text{(Eq 1)}$$

Here k is the specific heat ratio of the gas (1.4 for air and nitrogen, and 1.67 for helium), R_a is the specific gas constant that is defined as the relationship between the universal gas constant and the gas molecular weight. The Mach number is also used which is the relationship between the absolute gas velocity and the local sound speed.

$$M = \frac{v}{a}, \quad \text{where } a = \sqrt{kR_a T}. \quad \text{(Eq 2)}$$

Relationships existing between the speed coefficient and the Mach number allow for deriving equations using any of these numbers:

$$\lambda = \frac{M}{\sqrt{\frac{2}{k+1}\left(1 + \frac{k-1}{2} M^2\right)}}, \quad \text{(Eq 3)}$$

$$M = \frac{\lambda}{\sqrt{\frac{k+1}{2}\left(1 - \frac{k-1}{k+1}\lambda^2\right)}}. \quad \text{(Eq 4)}$$

Most equations are written more handily by using rather the velocity coefficient than the Mach number that is why this method is chosen for the present calculations.

The speed coefficient distribution along the nozzle is calculated as follows:

$$\frac{S_{cr}}{S(z)} = \lambda(z)\left(\frac{1 - b\lambda(z)^2}{1 - b}\right)^{\frac{1}{k-1}}, \quad \text{(Eq 5)}$$

here

$$b = \frac{k-1}{k+1}.$$

Note that the speed coefficient cannot be directly derived from this equation, thus, methods for finding roots of nonlinear equations must be employed. Based on the values of speed coefficient found, the remaining gas parameters can be easily determined using the following formulae:

$$\frac{T}{T_0} = 1 - b\lambda^2, \quad \text{(Eq 6)}$$

$$\frac{\rho}{\rho_0} = (1 - b\lambda^2)^{\frac{1}{k-1}}, \quad \text{(Eq 7)}$$

$$\frac{p}{p_0} = \left(\frac{\rho}{\rho_0}\right)^k. \quad \text{(Eq 8)}$$

Here T is the local gas temperature, ρ is the local gas density, p is the local pressure, parameters labeled by the index "0" are stagnation parameters. Note that isentropic flows are characterized by the conservation of stagnation parameters; hence, it is enough to calculate their values at the nozzle inlet and use them in further calculations as constants. In addition, pressure and temperature settled in the prechamber are usually fairly close to the gas stagnation pressure and temperature; therefore, it remains only to calculate the stagnation density by using the ideal gas state equation,

$$\rho = \frac{p}{R_a T}. \quad \text{(Eq 9)}$$

The above model can calculate accurately enough gas flow in relatively short well-profiled nozzles. To improve the accuracy of calculations with respect to the long nozzles that are characteristic of cold spray, it is necessary to take into account gas friction against the nozzle walls. This way, two models can be developed.

The first model is based on the problem of flow past a flat plate which is well studied, both experimentally and theoretically. It is known that under conditions of flow past a flat plate, a boundary layer starts growing on its front edge. For this case, a classical closed semi-empirical model is developed based on the Karman momentum equation written in the following form (Ref 16):

$$\frac{d\delta^{**}}{dz} = \frac{c_f}{2} - \frac{1}{v}\frac{dv}{dz}(2 + H - M^2)\delta^{**}. \quad \text{(Eq 10)}$$

Here δ^{**} is the momentum loss thickness, c_f is the friction coefficient which depends on the Reynolds number calculated taking into account the distance from the tip of the plate and the gas parameters, as well as the Mach

number, on the outer edge of the boundary layer. The gradient of parameters is taken into account by the Karman equation. The dependence of the friction coefficient on the Reynolds and Mach numbers is well defined by experiments whose results can be approximated as follows:

$$c_f = c_{f0}\frac{1-\xi}{\xi}\arcsin^2\sqrt{\xi}, \quad \text{(Eq 11)}$$

$$c_{f0} = 0.0263 Re_z^{-1/7}, \quad \text{(Eq 12)}$$

$$Re_z = \frac{\rho v z}{\mu}, \quad \text{(Eq 13)}$$

$$\xi = \frac{\frac{k-1}{2}M^2}{1+\frac{k-1}{2}M^2}. \quad \text{(Eq 14)}$$

The value equal to the relationship between the momentum loss thickness and the displacement thickness,

$$H = \frac{\delta^{**}}{\delta^*}, \quad \text{(Eq 15)}$$

is also defined by experiments and approximated by the expression

$$H = 1.4(1+0.3M^2). \quad \text{(Eq 16)}$$

Upon solving the Karman equation and finding momentum loss thickness, the corresponding displacement thickness is easily found

$$\delta^* = H\delta^{**}. \quad \text{(Eq 17)}$$

Let us consider the nozzle walls as a flat plate. The effect of the displacement thickness will be as follows: the flow parameters on the outer edge of the boundary layer starts changing in the way as if an ideal gas was flowing past a fictitious body whose walls are closer to each other by twice the displacement thickness. In this case, the flow in the nozzle is calculated in two main steps. First, gas parameters along the nozzle are calculated based on the isentropic flow equations, then, the displacement thickness is calculated using the parameters obtained. A fictitious nozzle is built whose each cross section area is calculated having in mind that its walls have become closer to each other by twice the displacement thickness. Further, the procedure is repeated until a balanced solution is obtained, i.e., gas parameters calculated on the outer edge of the boundary layer are in agreement with calculated values of the displacement thickness of the boundary layer.

The above model allow for calculating longer nozzles with a sufficient accuracy compared to calculations by the purely isentropic model that was used in the construction of this one only as an initial approximation.

The above relationships and algorithms are only sufficient for calculating particle motion near the nozzle axis. However, to calculate particle motion also at the periphery near the nozzle walls, it is required to calculate thickness of the boundary layer and to approximate velocity distribution and other gas parameters inside it. Experiments showed that, for a turbulent flow, the velocity profile inside the boundary layer can be estimated with a sufficient accuracy by using the following degree function:

$$\frac{\lambda}{\lambda_m} = \left(\frac{r}{\delta}\right)^n = \eta^n, \quad \text{at } n = 1/7. \quad \text{(Eq 18)}$$

Here, the r coordinate is the distance from the wall to the nozzle axis.

The relationship between the boundary layer thickness and the displacement thickness is given by a formula which simultaneously determines the displacement thickness:

$$\frac{\delta^*}{\delta} = 1 - \int_0^1 \frac{\rho\lambda}{\rho_m\lambda_m} d\eta. \quad \text{(Eq 19)}$$

As pressure transmitted from the main flow to the boundary layer remains the same, the density ratio can be replaced by the temperature ratio in accordance with the ideal gas state equation:

$$\frac{\rho}{\rho_m} = \frac{T_m}{T}. \quad \text{(Eq 20)}$$

On the other hand, if the nozzle walls are not purposely heated or cooled from the outside, the flow is characterized by a constant stagnation temperature. Then temperatures in the boundary layer are related by the Crocco integral through the relationship between velocity coefficients:

$$\frac{T}{T_m} = 1 + \frac{k-1}{2}M_m^2\left(1 - \left(\frac{\lambda}{\lambda_m}\right)^2\right). \quad \text{(Eq 21)}$$

The resulting formula for the boundary layer thickness has the form

$$\frac{\delta^*}{\delta} = 1 - \int_0^1 \frac{\lambda/\lambda_m}{1+\frac{k-1}{2}M_m^2\left(1-(\lambda/\lambda_m)^2\right)} d\eta. \quad \text{(Eq 22)}$$

In this integral, variable η can be easily substituted by the relationship between velocity coefficients $\bar{\lambda}$

$$\frac{\delta^*}{\delta} = 1 - \int_0^1 \frac{7\bar{\lambda}^7}{1+\frac{k-1}{2}M_m^2\left(1-\bar{\lambda}^2\right)} d\bar{\lambda}, \quad \text{(Eq 23)}$$

And, this formula can be rewritten using velocity coefficients

$$\frac{\delta*}{\delta} = 1 - 7\int_0^1 \frac{\left(1-b\lambda_m^2\right)\bar{\lambda}^7}{1-b\lambda_m^2\bar{\lambda}^2} d\bar{\lambda}. \quad \text{(Eq 24)}$$

Then, constancy of the stagnation temperature allows for calculating the static temperature

$$T(r) = T_0\left(1 - \frac{k-1}{k+1}\lambda^2(r)\right). \quad \text{(Eq 25)}$$

Cross-sectional constancy of the pressure is used to define the density based on the gas state equation

$$\rho(r) = p/RT(r). \quad \text{(Eq 26)}$$

In calculating even longer nozzles, a situation arises when the boundary layers grow to the point of reaching the nozzle axis, so to speak, they slam shut. In this case, a different model must be used which takes into account the nonisentropic character of the flow. Further down the flow path, the calculations were performed based on another gas dynamic model which is presented below.

The primary assumption is that the entire velocity profile is given by one and the same law "1/7" (18). The boundary layer thickness is assumed to be equal to the channel radius (junction of the boundary layers).

Accordingly to the laws of gas dynamics, transversal momentum flux $\int_S \rho\vec{v}v_n dS$ of a volume is equal to the forces exerted on this cross-sectional surface $\int_S p_n dS + \tau dS$. The gas velocity vector is fully convergent with the nozzle axis. Let us define the mass of gas flowing through the channel per unit time as $\dot{m} = G$.

Momentum $d(Gu)$ is influenced by the pressure force $[-(p_2S_2 - p_1S_1)]$ and the decelerating force of friction, F_{fr}. In addition, the walls generate an accelerating force linked to the increase of the nozzle transversal area pdS. By introducing a small increment of the longitudinal coordinate dz, the momentum conservation equation can be written as follows:

$$d(Gv) = -d(pS) + pdS - \tau U dz. \quad \text{(Eq 27)}$$

Here τ is the gas tangential stress and U is the channel perimeter.

Let us combine on the right-side terms denoting effects exerted on the flow: friction and channel widening,

$$d(Gv + pS) = pdS - \tau U dz. \quad \text{(Eq 28)}$$

The left side of the equation can be written as follows:

$$Gv + pS = G\left(v + \frac{p}{\rho v}\right). \quad \text{(Eq 29)}$$

Let us introduce the velocity coefficient in accordance with the expression $v = \lambda a_{cr}$, where a_{cr} depends only on the local gas stagnation temperature and, thus, is constant over all the channel for the adiabatic case:

$$Gv + pS = Ga_{cr}\left(\lambda + \frac{p}{\rho a_{cr}^2 \lambda}\right) \quad \text{(Eq 30)}$$

The following expression is obtained by using the ideal gas state equation:

$$\frac{p}{\rho a_{cr}^2} = \frac{RT}{a_{cr}^2} = \frac{a^2}{a_{cr}^2 k} = \frac{k+1}{2k} - \frac{k-1}{2k}\lambda^2. \quad \text{(Eq 31)}$$

Finally, a simple expression can be derived:

$$Cv + pS = \frac{k+1}{2k} Ga_{cr}\left(\lambda + \frac{1}{\lambda}\right). \quad \text{(Eq 32)}$$

Let us consider the right side of (27). Gas tangential stress is commonly expressed through velocity pressure:

$$\tau = c_f \frac{\rho v^2}{2} = c_f Ga_{cr} \frac{\lambda}{2S}. \quad \text{(Eq 33)}$$

The term pdS can be transformed and expressed through the product Ga_{cr} by introducing the gas dynamic function y:

$$y = \left(\frac{k+1}{2}\right)^{\frac{1}{k-1}} \frac{\lambda}{1 - \frac{k-1}{k+1}\lambda^2}, \quad \text{(Eq 34)}$$

$$pdS = \left(\frac{k+1}{2}\right)^{\frac{k}{k-1}} \frac{Ga_{cr}}{ky} \frac{dS}{S}. \quad \text{(Eq 35)}$$

Thus, equation for change in momentum (27) can be written in the form

$$\frac{k+1}{2k} d\left(Ga_{cr}\left(\lambda + \frac{1}{\lambda}\right)\right) = \left(\frac{k+1}{2}\right)^{\frac{k}{k-1}} \frac{Ga_{cr}}{ky} \frac{dS}{S} - c_f Ga_{cr} \lambda \frac{U}{2S} dz. \quad \text{(Eq 36)}$$

Let us introduce the channel hydraulic diameter calculated by the formula

$$D = \frac{4S}{U}, \quad \text{(Eq 37)}$$

and the effective length

$$\chi = \frac{8k}{k+1} \frac{L}{D_{cr}} c_{fcr}. \quad \text{(Eq 38)}$$

Upon transformations, the following expression is obtained:

$$(\lambda^2 - 1)\frac{d\lambda}{\lambda} = \left[2\sigma(1 - a\lambda^2) - \frac{\chi\lambda^2}{2}\right]\frac{d\bar{x}}{\bar{D}}, \quad \text{(Eq 39)}$$

here $\sigma = \bar{D}_{ex} - 1$.

The friction coefficient is governed by the Reynolds number which is defined through the hydraulic diameter and other flow parameters by the expression

$$Re_D = \frac{\rho u D}{\mu} = \frac{GD}{\mu S}. \quad \text{(Eq 40)}$$

The friction coefficient is calculated by the empirical formula (Ref 13).

$$c_f = \frac{0.08}{Re^{0.25}}. \quad \text{(Eq 41)}$$

Thus, the fundamentals of the model proposed for the gas flow within the nozzle can be determined as follows. The flow in the subsonic part of the nozzle is calculated according to the ideal gas model. Starting from the nozzle throat, the increase of the boundary layers along the nozzle walls is numerically defined by the Karman equation up to the point where the boundary layers slam shut. In this case, the stagnation pressure near the nozzle axis is preserved. Then, starting from the point of the boundary

layers junction, the calculation is performed by equations for the mean gas flow parameters. The axial parameter values are restored in accordance with the "1/7" velocity distribution law.

Isobaricity of the exhaustion of the jet is assumed in free-flow calculations. In this paper, the calculation was performed on the base of empirical relationships which can be found in classical references as Ref 13, 17.

An important aspect is the modeling of the stream flowing onto a target. Let us consider the impingement of a supersonic jet on a normally positioned target. The gas flow decelerates and starts backward in front of the target surface. The transition from supersonic to subsonic velocities takes place because of a shock occurring at a certain distance z_w from the target surface. A high-pressure and high-density gas layer appears between the target surface and the shock front surface. Apparently, small particles passing through this compressed layer will loose some of their velocity. The thicker the compressed layer, the greater will be the velocity loss.

It is quite difficult to determine the Mach number distribution in the compressed layer. In this paper, a well-known method of polynomial approximation is used in order to define Mach numbers and their derivations between two points. A point of reference is chosen at the jet axis at the location of the shock. The third-order polynomial satisfies the following boundary conditions:

past the shock front $z = 0$:

$$M = M_S \quad \text{and} \quad dM/dz = 0, \tag{Eq 42}$$

and on the target surface $z = z_w$:

$$M = 0 \quad \text{and} \quad dM/dz = -0.5M_S/z_w. \tag{Eq 43}$$

Most of the above is obvious. The latter condition derived on the basis of a great amount of experimental data (Ref 18, 19) denotes the uniformity of the velocity gradient at the point where the flow starts back. Uniformity means here that the velocity gradients are equal according to the conservation law for velocity circulation at the stagnation point, i.e., $\left|\frac{\partial M}{\partial y}\right| = \left|\frac{\partial M}{\partial z}\right|$. The velocity v can be replaced by M because v tends to zero at the turning point. The following dependency satisfies the boundary conditions mentioned above:

$$M = M_S \left(1.5(z/z_w)^3 - 2.5(z/z_w)^2 + 1\right). \tag{Eq 44}$$

A more accurate approximation will require a more accurate model of the stream and its impingement. Currently, no simple model exists which can take into account a wide-range variation of the whole set of parameters mentioned above. The situation is also complicated by nonstationary phenomena such as oscillations of the jet and a bow shock under conditions of a nonisobaric exhaustion. Calculation of such flows requires separate research efforts and is not of concern to this paper.

A number of essential limitations of this model must be mentioned which do not allow using it for calculation of any kind of nozzle and at any parameters:

- The assumption of isobaricity of the free jet exhaustion is valid for each given nozzle only in a narrow range of parameters at which so-called isobaric exhaustion is realized, i.e., the pressure in the free jet is close to the atmospheric one. In case of a substantial variation of parameters, for example, pressure increasing or decreasing, an isobaric exhaustion-based calculation would be incorrect.
- The possibility of the transformation of a supersonic flow into a subsonic one at the nozzle exit in case of very long nozzles and small pressures is not taken into account.

In accordance with the limitations above, it was proposed to verify the model within the range of parameters of its validity and, namely, for the case when the gas static pressure is close to the atmospheric one. Such exhaustion mode is widely used in cold spray (Ref 1), that is why the model was developed for calculation of the gas flow parameters corresponding to these conditions.

FLUENT was used to verify the present numerical procedure. Calculations were performed at the same parameters of the gas flow, the results were compared. An ideal compressible gas was used in the calculations. The flow field was characterized by means of a coupled explicit method. The RNG $\kappa - \varepsilon$ turbulence model available in FLUENT was used. Gas and nozzle parameters are presented in Table 1. The Laval nozzle parameters were chosen close to the experimental ones.

2.2 Particle Acceleration in the Gas Stream

The particle velocity in the stream was calculated by a well-known formula

$$m_p v_p \frac{dv_p}{dz} = C_x \frac{\rho(v - v_p)^2}{2} S_{mid}, \tag{Eq 45}$$

which contains the particle Mach number

$$M_p = \frac{v - v_p}{a} \tag{Eq 46}$$

and the particle Reynolds number

$$Re_p = \frac{(v - v_p)\rho d_p}{\mu}. \tag{Eq 47}$$

Table 1 Gas and nozzle parameters

Parameter	Value
Gas type	Air
Inlet pressure	21 bar
Outlet pressure	1 bar
Gas total temperature	700 K, 500 K
Throat diameter	3 mm
Exit diameter	6 mm
Spraying distance	30 mm
Length of the diverging part	100 mm
Length of the converging part	20 mm

The Henderson approximation for the sphere resistance coefficient was used to calculate C_x. This approximation takes into account the change of the gas parameters in movement and the difference between the particle and gas temperature (Ref 20). The particle effect on the gaseous phase was not taken into account. Calculations were carried out to determine the particle velocity along the nozzle axis and the free-flow velocity. The effect of the particle collisions with the nozzle walls and between themselves on the particle velocity was neglected.

2.3 Software

On the basis of the above model, software was developed allowing for calculations of the gas flow parameters and the particle parameters in a supersonic nozzle under cold-spray conditions.

The ITAM software is a Windows EXE file. The window for input/output simulation data is shown in Fig. 1.

The first menu of the window specifies geometric parameters of the conic nozzle: critical and outlet diameters, length of the converging and diverging parts, and distance from the nozzle exit to the target surface. An option is proposed to specify the barrel length that is the part the nozzle with a constant diameter equal to the exit diameter of the conical nozzle. The second menu of the window specifies gas parameters: type, stagnation pressure, stagnation temperature, and pressure in the environment where the gas is flowing to (by default, it equals 0.1 MPa). The third menu proposes to select particle parameters from a list containing the most commonly used metals as for example Al, Cu, Zn, Ni, Ti, etc., as well as nonmetallic materials: diamond, Al_2O_3, SiC, Teflon. It also sets the initial velocity and temperature of the particles at the moment of their injection into the nozzle, and the location of the injection point.

Some simulation data are displayed directly on the software panel. These are inlet and outlet velocity of the gas and particles, particle velocity at the impact on the substrate, particle temperature. Outlet gas pressure is also displayed in order to control the isobar character of the flow. This is necessary because, by default, the program assumes that the gas flows out of the nozzle at a pressure equal to the environment one. Simulation values can be saved in an ASCII file for importation into other software such as Excel, Origin, etc., to produce graphs.

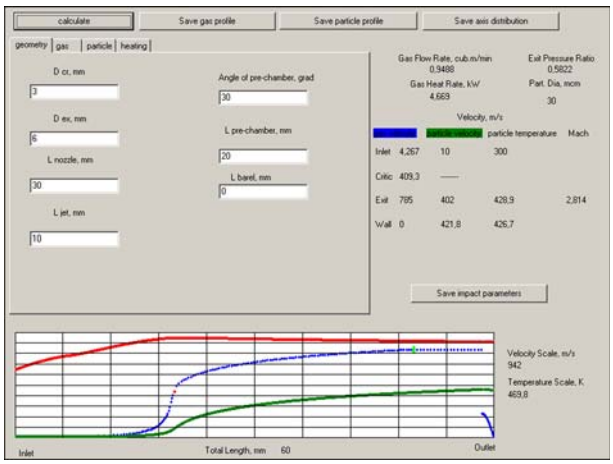

Fig. 1 Window of the ITAM software

3. Modeling of Collision-Induced Activation of Particles Moving in a Gas Dynamic Channel

When moving inside the gas dynamic channel, metallic particles are activated by collisions with abrasive particles.

Let us consider a certain volume of gas ΔV loaded with a number N_m of metallic particles and a number N_a of abrasive particles which is moving with a certain velocity inside a gas dynamic channel. A certain number α of collisions between metallic and abrasive particles occur per unit time. Let us assume that, at a certain moment of time, the given volume of gas contains N_m^* activated metallic particles, i.e., particles which have already been hit at least once by abrasive particles. Thus, αdt collisions will occur during the small time interval dt. The number of metallic-abrasive particle collision for each metal particle will be equal

$$I = \frac{\alpha dt}{N_m} \quad \text{(Eq 48)}$$

Based on the above number, the number of collisions with nonactivated metallic particles is equal to $\frac{N_m - N_m^*}{N_m}\alpha dt$. Thus, the increase of the number of activated particles is given by the following equation:

$$dN_m^* = \frac{N_m - N_m^*}{N_m}\alpha dt \quad \text{(Eq 49)}$$

$$dt = dz/v_{pm} \quad \text{(Eq 50)}$$

The next step is to estimate the number of collisions α per unit time. Let metallic and abrasive particles move along the nozzle axis at different velocities, the abrasive particle velocity being higher. In the system of coordinates of the metallic particles, the abrasive particles are traveling at a relative velocity $|v_{pa} - v_{pm}| = \Delta v_p$. During the small time interval dt, the abrasive particles cover the distance

$$dl = \Delta v_p dt. \quad \text{(Eq 51)}$$

S_{ex} denotes the area of a selected cross section of the channel. Let us suppose there is an abrasive particle in this cross section. Abrasive particles have a random distribution; therefore, the selected particle can be situated in any point of the cross section. With regard to the total of particles in the given gas volume, it can be assumed that all the abrasive particles N_a randomly pass through a cylinder with the thickness dl and the cross section area S_{ex}. As the cylinder contains $\frac{N_m}{\Delta V}S_{ex}dl$ metallic particles, the probability of collision is given be the relationship between the area of the collision and the cross section area

of the cylinder, i.e., $\frac{N_m}{\Delta V} S_{col} dl$. Here S_{col} is the area of collision of two particles,

$$S_{col} = \pi(d_{pm} + d_{pa})^2/4 \quad \text{(Eq 52)}$$

The number of collisions per unit time α is defined by the formula

$$\alpha = \frac{\pi}{4} \frac{N_a N_m}{\Delta V} \Delta v_p (d_{pm} + d_{pa})^2. \quad \text{(Eq 53)}$$

The value obtained is then introduced in the activation equation:

$$\frac{dN_m^*}{N_m} = \left(1 - \frac{N_m^*}{N_m}\right) \frac{\pi n_{pa} \Delta v_p (d_{pm} + d_{pa})^2}{4 v_{pm}} dz. \quad \text{(Eq 54)}$$

Here $n_{pa} = N_a/\Delta V$ is the numerical concentration of abrasive particles in the nozzle cross section expressed by the following formula using the mass flow of abrasive material:

$$n_{pa} = \frac{G_{pa}}{m_{pa} v_{pa} S_{ex}}, \quad \text{(Eq 55)}$$

where m_{pa} is the weight of a single abrasive particle.

The equation is solved by the integral

$$\frac{N_m^*}{N_m} = 1 - \exp\left(-\frac{G_{pa}\pi(d_{pm} + d_{pa})^2}{4 m_{pa}} \int_{L_0}^{L_1} \left|\frac{1}{v_{pa}} - \frac{1}{v_{pm}}\right| \frac{dz}{S_{ex}}\right). \quad \text{(Eq 56)}$$

Here $L_1 - L_0$ is the distance between the point of injection of abrasive particles and the nozzle exit, i.e., the distance along which metallic and abrasive particles interact with each other inside the nozzle.

In essence, the relationship $\frac{N_m^*}{N_m}$ expresses the probability of collision of a single metallic particle with an abrasive particle while traveling along the nozzle channel.

Let us introduce a symbol:

$$p = \frac{N_m^*}{N_m} \quad \text{(Eq 57)}$$

In this case, the following value

$$I = \left(-\frac{G_a \pi(d_{pm} + d_{pa})^2}{12 m_{pa}} \int_{L_0}^{L_1} \left|\frac{1}{v_{pa}} - \frac{1}{v_{pm}}\right| \frac{dz}{S_{ex}}\right) \quad \text{(Eq 58)}$$

seems to be nothing else, but the average number of collisions between metallic and abrasive particles.

It is obvious that the model of metallic/ceramic particle collision described here is only an approximation and does not take into account several aspects. One of them is the change of velocity of metallic and ceramic particles upon collision. Calculation of this phenomenon is undoubtedly one of the most important directions in refinement and optimization of the model. However, the assessment of the probability of metallic/ceramic particle collisions, as a preliminary step to studying particle collision-induced effects, can be performed by the model as presented above.

4. Calculation Results

4.1 Calculation of the Gas Flow

The calculation results for the gas velocity along the nozzle axis by the ITAM software and by FLUENT are presented in Fig. 2(a) and (b), within the distance form the nozzle inlet up to the substrate and within the stagnation distance in front of the substrate, respectively.

The graphs show a sufficient agreement between the modeling results by the ITAM software and by FLUENT. The latter predicts feeble diamond shocks. This is explained by the conical shape of the nozzle throughout its longitudinal cross section that determines the jet expansion up to the nozzle exit. In this case, feeble diamond shocks occur even at equal pressures at the nozzle exit section and in the surrounding atmosphere that was experimentally observed in Ref 13. Naturally, data on diamond shocks are not given by the ITAM software. It is evident that a change in the exhaustion mode whether in the direction of increasing or decreasing pressure will lead to the appearance of stronger diamond shocks and, thus,

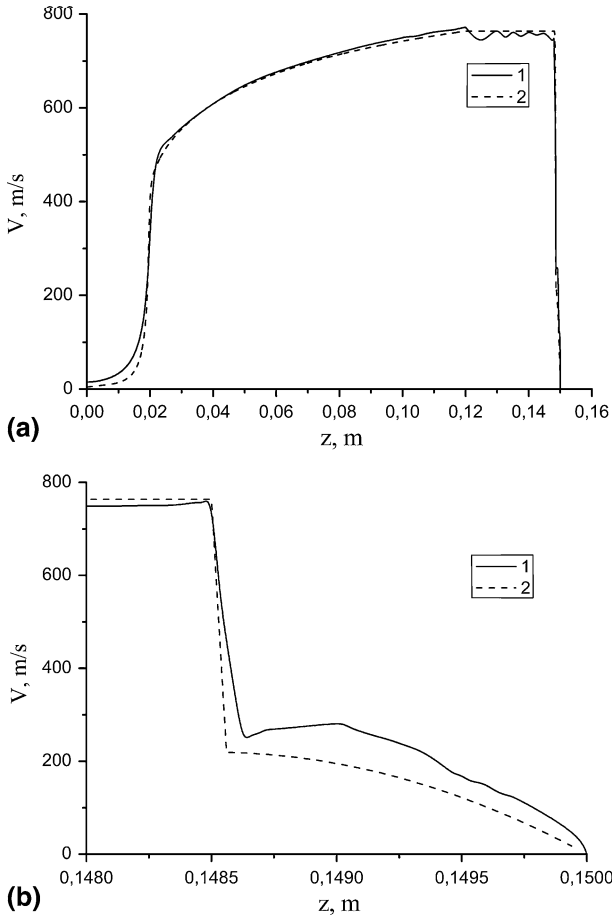

Fig. 2 Simulation values of gas velocity v along the nozzle axis z (a) within the distance form the nozzle inlet up to the substrate, and (b) within the stagnation distance in front of the substrate, gas pressure is 2.1 MPa, gas temperature is 500 K: (1) by FLUENT, (2) by ITAM software

to a greater divergence of the FLUENT and ITAM software modeling results.

Thus, the model developed and its computer-based application allow for calculating gas flow in supersonic nozzles with a satisfactory accuracy and provide a time saving of 2-3 orders of magnitude over FLUENT.

4.2 Particle Parameters. Probability of Collision

Velocity of metallic (aluminum and copper) and silicon carbide particles were calculated. Metallic particles were injected into the subsonic part of the nozzle ($z = 0$), and abrasive particles into different parts ($z = 0 \ldots 0.12$). Simulations coordinates of the points of SiC injection are indicated by arrows in Fig. 3.

Graphs in Fig. 4 and 5 represent the velocity distribution of abrasive and copper particles, and of abrasive and aluminum particles, respectively, when both powders were injected at the point $z = 0$.

The horizontal axis z corresponds to the nozzle length. The critical cross section (nozzle throat) is situated at a distance of 20 mm from the nozzle inlet. Here, a sharp acceleration of the gas and the particles can be observed. The gas-particle flow shows a smooth acceleration in the supersonic part (from 20 up to 120 mm). The substrate is situated at a distance of 30 mm from the nozzle exit that corresponds to the 150 mm coordinate in Fig. 4 and 5.

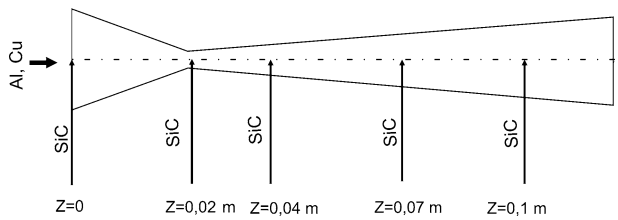

Fig. 3 Layout of the injection into the nozzle of metallic and abrasive powders

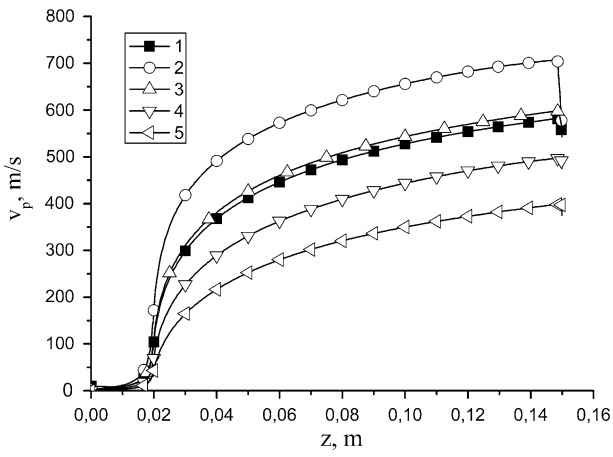

Fig. 4 Simulation values of aluminum and abrasive particles velocity v_p along the nozzle axis z, air stagnation temperature is 500 K, stagnation pressure is 2.1 MPa: (1) aluminum, (2) silicon carbide 5 μm, (3) SiC 15 μm, (4) SiC 45 μm, (5) SiC 135 μm

Graphs in Fig. 4 and 5 demonstrate that, depending on their size, abrasive particles can travel at higher or lower velocities compared to metallic ones. It is interesting to note that the impact velocities of 5 and 15 μm abrasive particles are close to each other due to the velocity loss by the small (5 μm) particles in the shock-compressed layer in front of the target. A further reduction of the size of abrasive particles would be ineffective because their impact velocity would diminish even more that, in turn, would also reduce the activation effect of abrasive particles on the substrate surface.

As discussed above, metallic particles during their motion may be activated by collisions with abrasive particles, thus, it is of great importance to calculate a characteristic relative velocity of the particles. Graphs in Fig. 6 and 7 represent relative velocity of abrasive particles with regard to aluminum and copper particles, respectively.

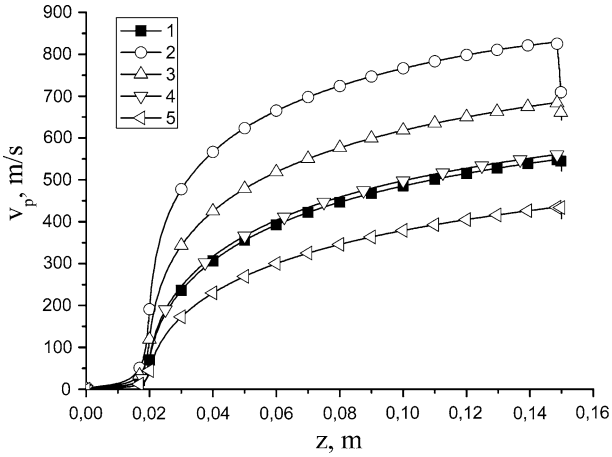

Fig. 5 Simulation values of copper and abrasive particles velocity v_p along the nozzle axis z, air stagnation temperature is 500 K, stagnation pressure is 2.1 MPa: (1) copper, (2) silicon carbide 5 μm, (3) SiC 15 μm, (4) SiC 45 μm, (5) SiC 135 μm

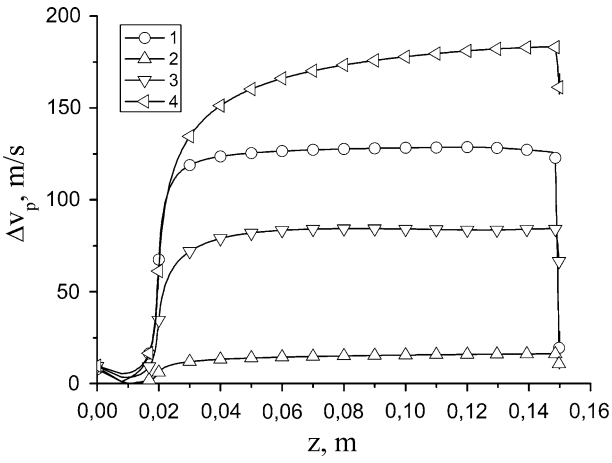

Fig. 6 Relative velocity of silicon carbide particles with respect to aluminum particles Δv_p along the nozzle axis z, air stagnation temperature is 500 K, stagnation pressure is 2.1 MPa: (1) silicon carbide 5 μm, (2) SiC 15 μm, (3) SiC 45 μm, (4) SiC 135 μm

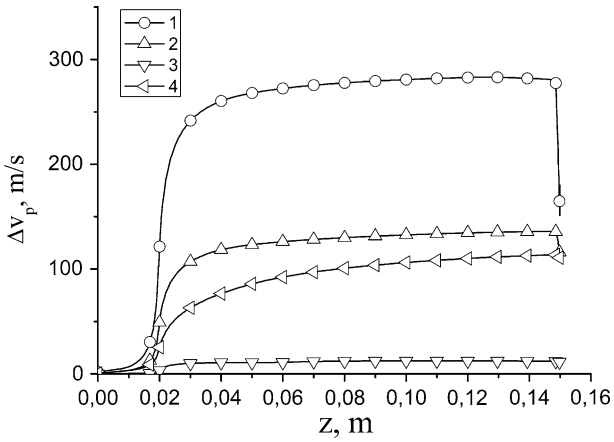

Fig. 7 Relative velocity of silicon carbide particles with respect to copper particles Δv_p along the nozzle axis z, air stagnation temperature is 700 K, stagnation pressure is 2.1 MPa: (1) silicon carbide 5 μm, (2) SiC 15 μm, (3) SiC 45 μm, (4) SiC 135 μm

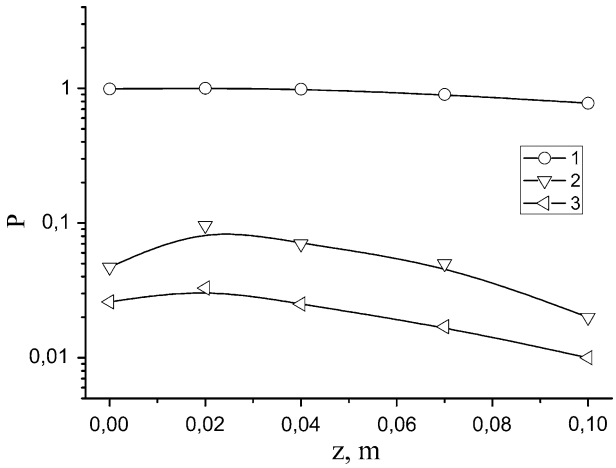

Fig. 8 Probability of the aluminum-abrasive paricle collision P vs. axial coordinate z of the point of the abrasive powder injection into the nozzle, air stagnation temperature is 500 K, stagnation pressure is 2.1 MPa: (1) silicon carbide 5 μm, (2) SiC 45 μm, (3) SiC 135 μm

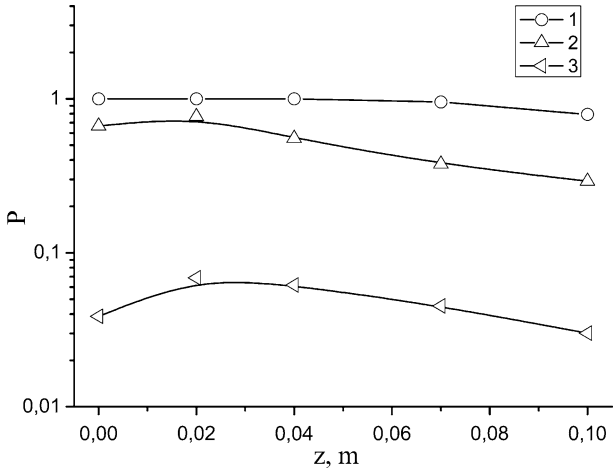

Fig. 9 Probability of the copper-abrasive paricle collision P vs. axial coordinate z of the point of the abrasive powder injection into the nozzle, air stagnation temperature is 700 K, stagnation pressure is 2.1 MPa: (1) silicon carbide 5 μm, (2) SiC 15 μm, (3) SiC 135 μm

Graphs in Fig. 6 and 7 show the presence of a characteristic spread in velocities of the mixture components along almost the whole length of the particle trajectory except in the beginning and in the end. The characteristic spread in velocities for the mixture of silicon carbide with aluminum is minor, while it is larger for the case of copper, from 40 up to 150 m/s and from 30 up to 300 m/s, respectively. From the point of view of the particle size, the highest spread in velocities was found for the mixture of aluminum particles with 5 and 135 μm SiC, and for the mixture of copper particles and 5 μm SiC.

Calculations were carried out for different points of the injection of abrasive particle varying form $z = 0$ up to $z = 0.12$ m. Based on the data obtained, the probability of collision between metallic and silicon carbide particles was estimated. The abrasive particle feed rate was 0.5 g/s, that is typical for cold spray. It is important to note that only collisions hard enough to provoke the metallic particle activation should be statistically taken into account, i.e., the difference in collision velocities should be superior to for example 50 m/s. Note that the value of 50 m/s was arbitrarily chosen as a starting point for the demonstration of the calculation method. It is clear that this value should be enough to cause some damage of the metallic particle surface upon collision, for example, to remove oxide film. However, the physical correctness of the choice of such value requires further research.

Thus, collisions occurred at smaller impact velocities were not statistically considered. It was the case of 15 and 45 μm SiC particles in the mixture with aluminum and copper, respectively, because of their low relative velocities during almost the whole trajectory.

The probability of collisions of aluminum and copper particles with different fractions of silicon carbide particles depending on the location of the point of abrasive particles injection into the nozzle was numerically estimated. The calculation results are presented in Fig. 8 and 9.

One can see from these graphs that 5 μm-sized abrasive particles are the most efficient for activation. The probability of collision between 5 μm-sized silicon carbide and metallic particles is practically equal to 1 for all the points of the abrasive powder injection into the stream. This means that, in average, each metallic particle collided with abrasive particles at least once. Along with this, it is evident that the greater is the number of collisions, the higher the level of activation. In other words, the number of collisions must be taken into account in order to comprehensively assess the interaction of metallic and abrasive particles. The graph in Fig. 10 represents the dependence of the number of collisions between 5 μm-sized silicon carbide and metallic (copper and aluminum) particles on the location of the point of powder injection.

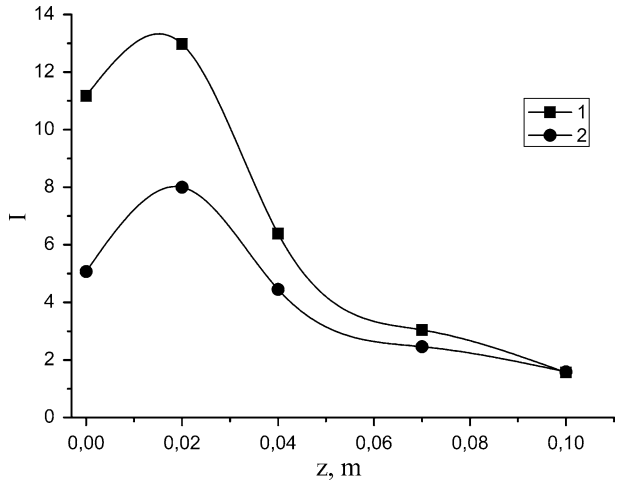

Fig. 10 Number of collisions between particles I vs. axial coordinate z of the point of the abrasive powder injection into the nozzle: (1) silicon carbide 5 μm and copper, gas temperature is 700 K, pressure is 2.1 MPa, (2) silicon carbide 5 μm and aluminum, gas temperature is 500 K, pressure is 2.1 MPa

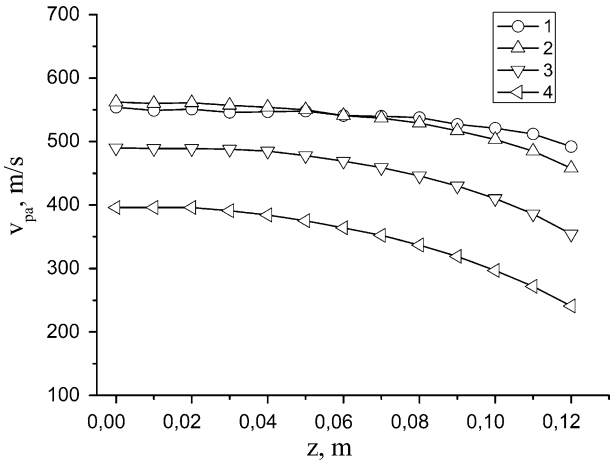

Fig. 11 Abrasive particle velocity v_p at the impact on the target surface vs. axial coordinate z of the point of the abrasive powder injection into the nozzle, air stagnation temperature is 500 K, stagnation pressure is 2.1 MPa: (1) silicon carbide 5 μm, (2) SiC 15 μm, (3) SiC 45 μm, (4) SiC 135 μm

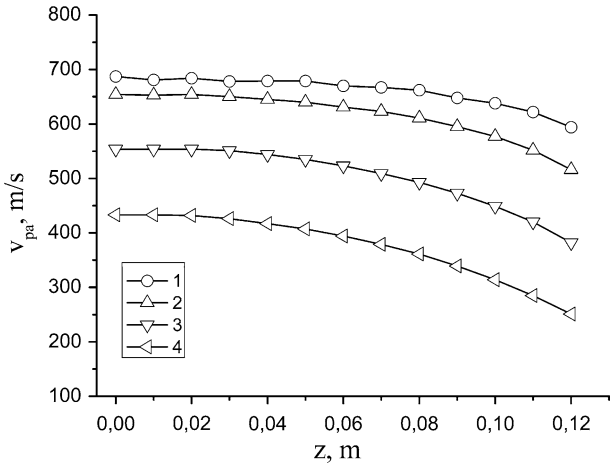

Fig. 12 Abrasive particle velocity at the impact on the target surface v_p vs. axial coordinate z of the point of the abrasive powder injection into the nozzle, air stagnation temperature is 700 K, stagnation pressure is 2.1 MPa: (1) silicon carbide 5 μm, (2) SiC 15 μm, (3) SiC 45 μm, (4) SiC 135 μm

One can see that the greatest number of collisions correspond to the case where silicon carbide particles are injected just past the nozzle throat. Therefore, regardless the fact that 5 μm-sized abrasive particles yield a high probability of collisions at any location of the point of their injection into the stream, the number of collisions—and, thus, the level of activation—is substantially dependent on the latter.

The probability of collisions decreases dramatically for the case of larger SiC particles, and its maximum corresponds to the zone situated just past the nozzle throat. The probability of collisions is the lowest for 135 μm SiC. It is logical to conclude that if the probability of collisions is minor, an analysis of the number of collisions will be useless. A first evident reason for such a sharp drop of the collision likelihood is the use of a constant mass feed rate of ceramics in the calculations. It is logical that the number of ceramic particles in the steam will diminish with their size at a constant mass feed rate. This explains the decrease of the collision likelihood.

As an example case, the probability of collisions was calculated for the 0.5 g/s feed rate of abrasive particles. With the increase of that value from G_{pa0} up to G_{pa}, the former will grow as well in accordance with the relationship

$$p(G_{pa}) = 1 - (1 - p_0)^{\frac{G}{G_{pa0}}} \quad \text{(Eq 59)}$$

One can therefore conclude that an appropriate value of feed rate may be chosen for abrasive particles of any size in order to assure a high probability of collisions. That is, aiming at this purpose, a suitable feed rate can be selected even for 135 μm-sized SiC particles.

It is important to mention, along with the activation of metallic particles during their motion in the nozzle, the activation of the substrate surface occurring due to a high-velocity impact of abrasive particles. The right choice of the point of powder injection into the stream should take into consideration both types of activation, i.e., research must be done to determine if a location selected will assure an equally high level of activation for metal particles and for the substrate surface. In this purpose, the impact velocity of silicon carbide particles was calculated for different points of their injection into the nozzle under conditions typical for cold spray. The calculations were carried out under conditions typical for cold spraying aluminum and copper, Fig. 11 and 12, respectively.

The calculations showed that the closer to the nozzle exit is the point of the abrasive powder injection, the lower the impact velocity of the particles. This dependence is

valid for all the range of the particle sizes studied. Altogether, the absolute value of the impact velocity remains high and reaches above 200 m/s even for the largest particles. Hence, the location of the point of the abrasive powder injection is not a significant factor in the level of activation of the substrate surface by the high-velocity impact of abrasive particles.

5. Discussion

As mentioned above, currently the main mechanism responsible for the increase of the deposition coefficient under the addition of ceramic particles into the stream is thought to be the activation of the substrate surface by the high-speed impact of the ceramic particles. Unfortunately, it is not currently clear how to experimentally analyse the real extent to which the activation of metal particles by collisions with ceramics is effective (and even if such effect really exists), especially in comparison with the activation of the surface due to impact. It is impossible to experimentally separate these two types of activation (activation of the surface and of the colliding particles) as they always occur simultaneously in the spraying process. For example, the calculations presented above show that an increase of the particle concentration in the stream increases the probability of particle collisions in it and, thus, their activation by collisions. On the other hand, the increased particle concentration may also change the surface erosion-activation parameters in an unpredictable way, and, thus, blur the result of the activation effect in the stream.

In any case, to build a detailed picture of the process of spraying metal-ceramic mixtures and of related processes of surface activation, activation by collisions and due to erosion requires further theoretical and experimental research.

It should be emphasized one more time that the ambition of the present study was not to provide a complete and comprehensive analysis of the process of metallic-ceramic particle collision. The aim of this work was to conduct preliminary assessments of the likelihood of such collisions and of the hypothesis of the metal particle activation due to these collisions.

6. Conclusions

A model of gas flow in cold spray nozzles was proposed and successfully applied in calculations. Based on this model, ITAM software was developed especially for numerical simulation of cold spray process. The result obtained were verified by FLUENT and showed a satisfactory accuracy of the ITAM software.

For the first time, a mathematical model takes into account the interaction of metallic and abrasive particles inside the nozzle. The assessment of the degree of interaction allows for estimating the level of activation of metallic powder by abrasive powder. Using the model and the software developed, parameters of aluminum and copper powders and of four different fractions of silicon carbide powder were calculated, the probability of collision between metallic and abrasive particles and the number of collisions were estimated. It was established that, for the same abrasive powder feed rate, the probability of collision and the number of collisions are by orders of magnitudes higher for the small abrasive particles compared to the large fractions. It was also found that the separate injection of metallic and abrasive particles into the nozzle is favorable for the intensification of collisions, the optimal solution being to inject abrasive particles in the zone just past the critical cross section of the nozzle.

Acknowledgment

The study was supported by the Russian Foundation for Basic Research (Grants No 08-01-00108a and No 09-08-00543a).

References

1. A. Papyrin, V. Kosarev, S. Klinkov, A. Alkhimov, and V. Fomin, *Cold Spray Technology*, Elsevier Science, Amsterdam, 2007, p 336
2. T. Schmidt, F. Gaertner, H. Assadi, and H. Kreye, Development of a Generalized Parameter Window for Cold Spray Deposition, *Acta Mater.*, 2006, **54**, p 729-742
3. M. Grujicic, C.L. Zhao, W.S. DeRosset, and D. Helfritch, Adiabatic Shear Instability Based Mechanism for Particles/Substrate Bonding in the Cold-Gad Dynamic-Spray Process, *Mater. Design*, 2004, **25**, p 681-688
4. H. Assadi, F. Gaertner, T. Stoltenhoff, and H. Kreye, Bonding Mechanism in Cold Gas Spraying, *Acta Mater.*, 2003, **51**, p 4379-4394
5. A. Shkodkin, A. Kashirin, O. Klyuev, and T. Buzdygar, Metal Particle Deposition Stimulation by Surface Abrasive Treatment in Gas Dynamic Spraying, *J. Therm. Spray Technol.*, 2006, **15**, p 382-385
6. R. Maev and V. Leshchynsky, *Introduction to Low Pressure Gas Dynamic Spray: Physics & Technology*, Wiley-VCH, Weinheim, 2008, p 234
7. R.G. Maev and V Leshchynsky, Air Gas Dynamic Spraying in Powder Mixtures: Theory and Application, *J. Therm. Spray Technol.*, 2006, **15**, p 198-205
8. H.Y. Lee, S.H. Jung, S.Y. Lee, Y.H. You, and K.H. Ko, Correlation Between Al_2O_3 Particles and Interface of Al-Al_2O_3 coatings by cold spray, *Appl. Surf. Sci.*, 2005, **252**, p 1891-1898
9. A. Papyrin, V. Kosarev, S. Klinkov, A. Sova, I. Smurov, and P. Bertrand, Investigation of Composites: Metal—Ceramics and Metal—Metal Coatings Produced with Cold Spray Equipment with Ejector, *Thermal Spray Crossing Borders: Proceedings of the 2008 International Thermal Spray Conference*, E. Lugscheider, Ed., June 2-4, 2008 (Maastricht, Netherlands), ASM International, 2008
10. T.-C. Jen, L. Li, W. Cui, Q. Chen, and X. Zhang, Numerical Investigations on Cold Gas Dynamic Spray Process with Nano- and Microsize Particles, *Int. J. Heat Mass Transf.*, 2005, **48**, p 4384-4396
11. W.-Y. Li, H. Liao, G. Douchy, and C. Coddet, Optimal Design of a Cold Spray Nozzle by Numerical Analysis of Particle Velocity and Experimental Validation with 316L Stainless Steel Powder, *Mater. Design*, 2007, **28**, p 2129-2137
12. W.-Y. Li, H. Liao, H.-T. Wang, C.-J. Li, G. Zhang, and C. Coddet, Optimal Design of a Convergent-Barrel Cold Spray Nozzle by Numerical Method, *Appl. Surf. Sci.*, 2006, **253**, p 708-713

13. G.N. Abramovich, *Applied Gas Dynamics,* Nauka, Moscow, 1976, p 824 (in Russian)
14. R.C. Dykhuizen and M.F. Smith, Gas Dynamic Principles of Cold Spray, *J. Therm. Spray Technol.*, 1998, **7**(2), p 205-212
15. M. Grujicic, C.L. Zhaoa, C. Tonga, W.S. DeRosset, and D. Helfritch, Analysis of the Impact Velocity of Powder Particles in the Cold-Gas Dynamic-Spray Process, *Mater. Sci. Eng.*, 2004, **368**, p 222-230
16. G. Schlichting, *Theory of Boundary Layer*, Nauka, Moscow, 1974, p 742 (in Russian)
17. M.E. Deich and A.E. Zaryankin, *Gas Dynamic of Diffusors and Exhaust Hood*, Energiya, Moscow, 1970, p 384 (in Russian)
18. I.A. Belov, I.P. Ginzburg, and L.I. Shoob, Supersonic Underexpanded Jet Impingement Upon Flat Plate, *Int. J. Heat Trans.*, 1973, **16**, p 2067-2076
19. T. Nakatogawa, M. Hirata, and I. Kukita, Desintegration of a Supersonic Jet Impinging Normally on a Flat Plate, *J. Spacecraft*, 1971, **8**(4), p 410-411
20. C.B. Henderson, Drag Coefficient of Spheres in Continuum and Rarefied Flows, *AIAA J.*, 1976, **14**, p 707-708